


ISSN: 0095-8972 (Print) 1029-0389 (Online) Journal homepage: <http://www.tandfonline.com/loi/gcoo20>


A thiosemicarbazone copper(II) complex as a potential anticancer agent

Zhong-Ying Ma, Jia Shao, Wei-Guo Bao, Zhao-Yan Qiang & Jing-Yuan Xu


To cite this article: Zhong-Ying Ma, Jia Shao, Wei-Guo Bao, Zhao-Yan Qiang & Jing-Yuan Xu (2015) A thiosemicarbazone copper(II) complex as a potential anticancer agent, Journal of Coordination Chemistry, 68:2, 277-294, DOI: [10.1080/00958972.2014.979811](https://doi.org/10.1080/00958972.2014.979811)

To link to this article: <http://dx.doi.org/10.1080/00958972.2014.979811>

 View supplementary material 

 Accepted author version posted online: 24 Oct 2014.
Published online: 27 Nov 2014.

 Submit your article to this journal 

 Article views: 129

 View related articles 

 View Crossmark data 

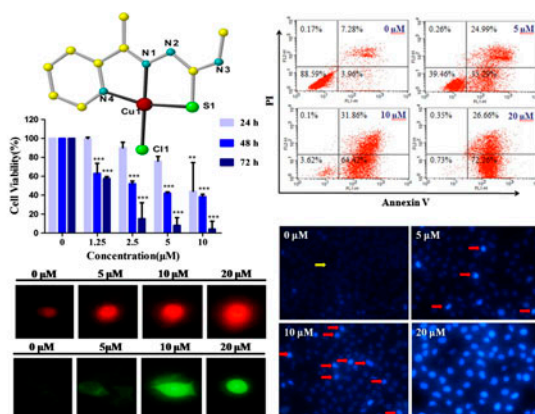
 Citing articles: 2 View citing articles 

A thiosemicarbazone copper(II) complex as a potential anticancer agent

ZHONG-YING MA^{1,†}, JIA SHAO^{1,†}, WEI-GUO BAO[†], ZHAO-YAN QIANG^{*‡} and JING-YUAN XU^{*†}

[†]Tianjin Key Laboratory on Technologies Enabling Development of Clinical Therapeutics and Diagnostics (Theranostics), School of Pharmacy, Tianjin Medical University, Tianjin, China
[‡]School of Basic Medicine, Tianjin Medical University, Tianjin, China

(Received 17 July 2014; accepted 25 September 2014)



Thiosemicarbazone Cu(II) complex exhibited great growth inhibition and induction of apoptosis in HeLa cells via oxidative DNA damage pathway which can act as a potential anticancer agent.

The preparation and the structure of a copper(II) complex, [Cu(4ML)Cl] (**1**) (H4ML = 2-acetylpyridine-4-methylthiosemicarbazone), are described. Complex **1** crystallizes in a monoclinic $P2_1/c$ space group with $a = 7.977(2)$ Å, $b = 15.824(5)$ Å, $c = 9.126(2)$ Å, $\alpha = \gamma = 90^\circ$, $\beta = 91.974(2)^\circ$, $V = 1151.26(5)$ Å³, $Z = 4$, $F(0\ 0\ 0) = 620$. According to X-ray crystallographic studies, each Cu(II) ion lies in a square planar coordination geometry based on the 4ML⁻ and Cl⁻ ligands. The complex displayed excellent inhibitory activity against various tumor cells (HeLa, HepG-2 and SGC-7901), offering lower IC₅₀ value of 3.2 ± 0.7 µM than cisplatin (10 ± 2 µM) on HeLa cells at 48 h. Complex **1** could significantly suppress HeLa cell viability in a dose-dependent manner. Flow cytometric analysis showed that **1** induced HeLa cell apoptosis, which might be associated with cell cycle arrests at S and G2 phases. Consistent with results of DNA cleavage experiments, comet assay indicated that **1** caused severe DNA fragmentation. The production of ROS was elevated with increasing concentration of **1**, suggesting that **1** was capable of promoting HeLa cell apoptosis through an oxidative DNA damage pathway.

*Corresponding authors. Email: qzyss@sina.com (Z.-Y. Qiang); xujingyuan@tmu.edu.cn (J.-Y. Xu)

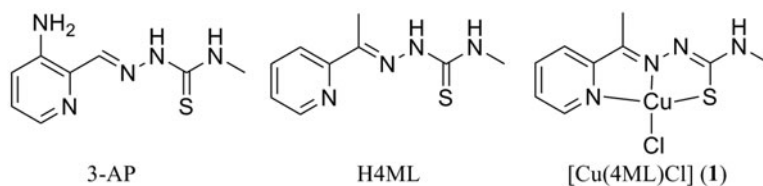
¹These authors contributed equally to this work.

Keywords: Thiosemicarbazone; Copper(II) complex; Anticancer; Apoptosis; Biological evaluation

1. Introduction

Metal-containing drugs have been explored for decades, and cisplatin is one of the most effective anticancer chemotherapy agents against a wide variety of solid tumors [1–4]. However, cisplatin recipients often acquire resistance [5] by increased DNA-repair capacity in damaged cells, which diminishes the efficacy of the drug. The conventional bifunctional anticancer Pt-drugs, such as cisplatin, carboplatin, and oxaliplatin, contain two reactive sites crosslinking intra- or inter-strand DNA, whereas the new class of monofunctional platinum anticancer agents with only one leaving group has been developed for their particular advantages. Lippard and co-workers reported monofunctional DNA adducts of pyriplatin [cis-diamminepyridinechloroplatinum(II)] inhibited transcription while significantly eluding repair, and its analog phenanthriplatin, cis-[Pt(NH₃)₂(phenanthridine)Cl]NO₃, exhibited higher efficacy than cisplatin in the established human cancer cell lines [6]. The distinct features of pyriplatin and its analogs strongly promote further research of monofunctional compounds as anticancer drug candidates. It makes sense to design, synthesize, and characterize new potential monofunctional metal-based antitumor agents to improve antitumor activity and reduce resistance of platinum-based drugs, and to investigate the possible molecular mechanism.

Copper complexes of thiosemicarbazone (TSC) and derivatives provide a series of non-platinum compounds with antitumor potential, which could be traced back to the early 1960s [7]. Some early work demonstrated interesting compounds with selective activity against tumors and low toxicity to normal cells by modifying the structure of TSC [8]. As an essential trace element, copper is important for most living species [9], involved in various kinds of important biological functions in cells, such as cellular trafficking, substrate oxidation, and redox regulation [10–14]. Copper(II) can significantly propagate reactive oxygen species (ROS) which further affects the development of cancer [15] as well as the potential manifestation of cytotoxicity [16, 17]. Some studies showed that influx and efflux of platinum-based antitumor agents are also regulated by transporters that control intracellular copper homeostasis [18, 19]. It probably strikes the mechanism of resistance to platinum-based antitumor agents from the aspect of transport system. For over 30 years, TSC have attracted interest [20] for their versatile multidentate coordination to metal ions and broad profile in pharmacological activity [21–27]. TSC has been evaluated as antiviral, antibacterial and anticancer therapeutics, and its biological activities arise from parent aldehyde or ketone moiety [28–39]. For example, 3-amino pyridine carboxaldehyde thiosemicarbazone (3-AP) (scheme 1), a well-known TSC member, is a potent ribonucleotide reductase



Scheme 1. 3-AP, H4ML and [Cu(4ML)Cl] (1).

inhibitor that is currently in phase II clinical trials for the treatment of various tumors, including non-small-cell lung cancer and renal carcinoma [40, 41].

In this article, we report the synthesis of a monofunctional copper(II) complex with TSC, [Cu(4ML)Cl] (**1**) (scheme 1), which exhibits oxidation-promoting activity through generating ROS. In order to evaluate its biological activities, cytotoxicity, apoptosis induction, and DNA damage, were employed. Our results show that **1** could effectively inhibit proliferation and induce apoptosis in human cervical cancer (HeLa) cells, presenting potential antitumor mechanisms.

2. Experimental

2.1. Materials and instrumentation

All reagents were obtained from commercial sources. 1-(Pyridin-2-yl)ethanone was purchased from Aladdin. Ethidium bromide (EB) and pUC19 DNA, 3-(4,5-dimethylthiazol-2-yl)-2,5-diphenyltetrazolium bromide (MTT), crystal violet, Hoechst 33342 and propidium iodide (PI) were purchased from Sigma. Fetal bovine serum (FBS) was purchased from Hyclone. DMEM medium was purchased from Gibco. Annexin V-FITC/PI assay kit was purchased from Jiamay Biotech. ROS assay kit was purchased from Beyotime. IR spectra were recorded on a Nicolet 380 spectrometer as KBr pellets from 4000–375 cm^{-1} with OMNIC software. $^1\text{H}/^{13}\text{C}$ NMR measurements were recorded on a Bruker UltraShield spectrometer. ESI-MS was analyzed using an Agilent MS instrument with an ion spray source using electrospray ionization in the positive-ion mode. Single crystal data were collected on a Rigaku Saturn X-ray CCD diffractometer using $\text{MoK}\alpha$ radiation at room temperature. The Gel Imaging and Documentation DigiDoc-It System were assessed using England Labworks Imaging and Analysis Software.

2.2. Synthesis of 2-acetylpyridine-4-methylthiosemicarbazone (H4ML)

The H4ML was prepared as reported [42–44]. A solution of 4-methylthiosemicarbazide (5 g, 0.048 M) in 80 mL of hot water was slowly added to a solution of 2-acetylpyridine (5.8 g, 0.048 M) in 40 mL ethanol with acetic acid (3–4 drops). The reaction mixture was refluxed for 2 h, and upon cooling afforded a white crystalline solid which was filtered off and recrystallized from ethanol. Yield: 91%, m.p. 175–177 °C. Selected IR data (KBr, cm^{-1}): 3288, 32400, 3043, 2967, 2901, 1578, 1537, 1438, 1432, 1407, 1291, 1231, 1148, 1107, 1072, 1036, 987, 903, 832, 778, 742, 681.5, 620, 572, 540. ^1H NMR (DMSO- d_6 , δ /ppm): 10.33 (s, 1H, NH), 8.62 (q, 1H, NH), 8.58 (d, 1H), 8.42 (d, 1H), 7.81 (td, 1H), 7.38 (td, 1H), 3.03 (d, 3H), 2.39 (s, 3H). ^{13}C NMR (DMSO- d_6 , δ /ppm): 178.7 (C7), 154.7 (C5), 148.4 (C1), 147.8 (C6), 136.3 (C3), 123.8 (C2), 120.7 (C4), 31.3 (C8), 12.1 (C9).

2.3. Synthesis of [Cu(4ML)Cl] (**1**)

A solution of $\text{CuCl}_2 \cdot 2\text{H}_2\text{O}$ (0.136 g, 0.8 mM) in MeOH (20 mL) was mixed with a solution of H4ML (0.167 g, 0.8 mM) in CHCl_3 (15 mL). The blue solution turned green immediately after adding drops of TEA. The resulting solution was stirred at ambient temperature for 3 h, followed by filtration to remove the insoluble materials. The filtrate was allowed to

stand at room temperature for one week resulting in formation of dark blue needle-like crystals suitable for X-ray diffraction analysis. The products were collected after washing with diethyl ether. Yield: 62 mg (ca. 25.38% based on Cu), m.p. > 250 °C. $C_9H_{11}ClCuN_4S$: calcd. C 35.29, H 3.62, N 18.29%; found C 35.56, H 3.48, N 18.11%. Selected IR data (KBr, cm^{-1}): 3836, 3741, 3307, 2963, 1598, 1562, 1524, 1499, 1458, 1400, 1334, 1250, 1194, 1163, 1079, 1043, 828, 771, 739, 646, 599, 562, 535, 491, 439. ESI-MS: $[M - Cl]^{+}$ displayed a peak at m/z 269.9995 (calcd 270.00) in MeOH.

2.4. X-ray crystallographic studies

A single crystal was placed on a Rigaku Saturn X-ray CCD diffractometer with $MoK\alpha$ radiation by using the ω -scan technique at room temperature (293 ± 1 K). Data collection and reduction were carried out with CrystalClear (Rigaku). The data were corrected for Lorentz and polarization effects. The structure was solved by direct methods SHELXS-97 [45] and refined on $|F|^2$ using the SHELXTL program package [46]. All non-hydrogen atoms were subjected to anisotropic refinements. The hydrogens included at the calculated positions were refined isotropically using a riding model.

2.5. DNA cleavage activities

Supercoiled DNA (100 ng) was used to study DNA cleavage activity of Cu(II) complex by agarose gel electrophoresis experiment. Complex **1** in DMF (10^{-2} M) was diluted using triple-distilled water to concentration of 10^{-3} M. Varied concentrations of **1** were added to supercoiled DNA and incubated at 37 °C for 4 h. After adding loading buffer, the samples in Tris-HAc/EDTA buffer were electrophoresed for 30 min at 85 V on 1% agarose gel. Finally, bands were observed by UV and photographed.

2.6. Cell lines and culture conditions

Human cervical cancer cell line HeLa and human liver hepatocellular carcinoma cell line HepG-2 were obtained from the American Type Culture Collection (Rockville, MD, USA). Human gastric cancer cell line SGC-7901 was purchased from China Center for Type Culture Collection (CCTCC). Cells were maintained in DMEM medium which was supplemented with 100 units mL^{-1} penicillin, 100 $\mu g mL^{-1}$ streptomycin, and 10% FBS; and grown at 37 °C in a humidified atmosphere containing 95% air and 5% CO_2 .

2.7. Cell viability assay

Cell viability was examined by MTT assay. Cells (HeLa, HepG-2 and SGC-7901) were seeded in 96-well plates and treated with test compound at concentrations of 0, 1.25, 2.5, 5, and 10 μM (0, 6.25, 12.5, 25, and 50 μM for $CuCl_2$ and H4ML). After exposure for 24, 48, and 72 h, 20 μL of 5 $mg mL^{-1}$ MTT in phosphate buffered saline (PBS, pH 7.4) was added to each well. The plates were incubated at 37 °C for a further 4 h. Thereafter, the supernatant was removed and the formazan product formed by viable cells was dissolved in 100 μL of DMSO. The absorbance of samples at 570 nm was recorded with an Enzyme-linked Immunosorbent Assay reader.

2.8. Cell clonogenic assay

Cells were seeded into a 6-well plate at a density of 300 cells per well. On the third day, cells were exposed to **1** (0, 0.3125, 0.625, 1.25, 2.5, and 5 μM) and incubated for 24 h. Two weeks later, cells were fixed with methanol–acetic acid (3 : 1) solution for 15 min. Then, they were stained with 1% crystal violet solution for 25 min. Finally, colonies were counted and the numbers of colonies in treated groups were expressed as a percentage of those in control group.

2.9. Hoechst 33342 staining

To investigate the apoptosis induction effect of **1**, the samples were analyzed by DNA-binding fluorochrome Hoechst 33342 staining. Cells (8×10^3) were incubated with **1** at 0, 5, 10, and 20 μM for 24 h. Then, cells were treated with Hoechst 33342 ($1 \mu\text{g mL}^{-1}$) at 37 °C for 15 min in the dark. After a further wash with PBS, samples were observed with the aid of fluorescence microscopy (Nikon ECLIPSE Ti).

2.10. Annexin V-FITC/PI analysis

According to manufacturer's instructions, 5×10^5 cells were exposed to various concentrations (0, 5, 10 and 20 μM) of **1**. Twenty four hours later, cells were harvested and washed with PBS. Afterwards, cells were resuspended in the $1 \times$ binding buffer (300 μL) and Annexin V-FITC (5 μL) was added to the cells and incubated for 15 min in the dark at room temperature. Then, cells were incubated for 5 min by PI (5 μL). Finally, after additional $1 \times$ binding buffer (200 μL), the samples were examined with BD FACSCalibur flow cytometry and data analysis was carried out with BD CellQuest™ Pro (version 5.2) software.

2.11. ROS production

As a cell-permeable indicator for ROS, the fluorescent probe DCFH-DA was used to measure ROS formation. Cells were seeded in a 12-well plate at a density of 8×10^4 . After exposure to different concentrations of **1** (0, 5, 10, and 20 μM) for 24 h, the cells were incubated with 1 μM DCFH-DA in DMEM medium at 37 °C in the dark for 30 min. Cells were then washed with PBS three times to remove DCFH-DA, which had not entered into the cells. The fluorescence was visualized immediately at wavelength of 485 nm for excitation and 525 nm for emission by an inverted fluorescence microscope (Nikon ECLIPSE Ti).

2.12. Single cell gel electrophoresis assay (comet assay)

Single cell gel electrophoresis or comet assay is a simple, sensitive, and rapid method for the detection and quantification of DNA damage. First, cells at a density of 7.5×10^4 exposed to **1** (0, 5, 10, and 20 μM) for 24 h were suspended in 0.65% low melting agarose and then spread over a window microscopic slide. The slides were precoated with 1 mL of 1% normal-melting agarose in PBS. They were left at 4 °C to solidify the low melting agarose. Then, the slides were placed in cold lysis solution (pH = 12) containing 2.5 M sodium chloride NaCl, 100 mM EDTA sodium salt Na_2EDTA , 10 mM Tris, and 1% Triton X-100 overnight at 4 °C. To allow uncoiling of DNA, the slides were kept in the high pH buffer

(300 mM NaOH and 1 mM Na₂EDTA) for 30 min. Subsequently, electrophoresis was carried out for 30 min at 300 mA at 4 °C. Thereafter, the slides were rinsed with neutralizing buffer (0.4 M Tris–HCl, pH 7.5) three times. Slides were buried in dehydrated ethanol for 30 min and naturally dried before staining with 10 µg mL⁻¹ EB solution. The samples were examined with a fluorescence microscope (Nikon ECLIPSE Ti) equipped with an excitation filter of 515–560 nm and a barrier filter of 590 nm.

2.13. Flow cytometry analysis of DNA content

5×10^5 HeLa cells were plated and exposed to medium which contained **1** at 0, 5, 10 and 20 µM for 24 h. Treated cells were harvested in cold PBS and fixed in 70% EtOH overnight at 4 °C. Then, cells were washed with PBS and digested by RNase A (0.25 mg mL⁻¹) for 30 min at 37 °C, followed by staining with PI (50 mg mL⁻¹) in the dark at room temperature for 30 min. The samples were analyzed with the BD FACSCalibur flow cytometry using CellQuest software to determine cell cycle distribution.

2.14. Statistical analysis

Data were presented as mean ± standard deviation (SD) unless otherwise stated. Statistical significance was performed by one-way ANOVA an assessment of differences using SPSS software (version 13.0). Differences were considered significant when $p < 0.05$, compared with the control group. Data shown was a representative of three independent experiments.

3. Results and discussion

3.1. Synthesis and characterization

H4ML and its copper(II) complex [Cu(4ML)Cl] (**1**) were synthesized and characterized by IR and ESI-MS techniques. The chief IR bands of free H4ML and complex from 4000–400 cm⁻¹ are listed and assigned. For the ligand, $\nu(-C=N)$ was observed at 1578 cm⁻¹, and two peaks of $\nu(NH)$ were found at 3288 and 3240 cm⁻¹, respectively. For **1**, only one $\nu(NH)$ was observed at 3307 cm⁻¹, indicating that the proton of one –NH group might be lost in formation of coordination compound. This also can be proved by the X-ray crystallographic studies. The typical peak shifted to lower frequencies from H4ML to **1**. The typical $\nu(C=N)$ at 1578 cm⁻¹ shifted to higher frequencies. The Cu(II) complex, with the deprotonated thiosemicarbazone arm, showed only one strong peak instead of two in the $\nu(NH)$ region. Deprotonation is likely to result in the frequency of this remaining band increasing. ESI-MS of **1** dissolved in a chromatography methanol solution was analyzed using an Agilent MS instrument with an ion spray source using electrospray ionization in positive-ion mode. ESI-MS indicated the presence of a prominent $[M - Cl]^{+}$ peak in the mass spectra of the Cu(II) complex corresponding to loss of the chloride (figure S1, see online supplemental material at <http://dx.doi.org/10.1080/00958972.2014.979811>). Complex **1** crystallizes in a monoclinic system with space group $P2_1/c$ and exhibited a neutral square planar coordination geometry just like cisplatin (figure 1). Each Cu was four-coordinate, by virtue of two nitrogens and one

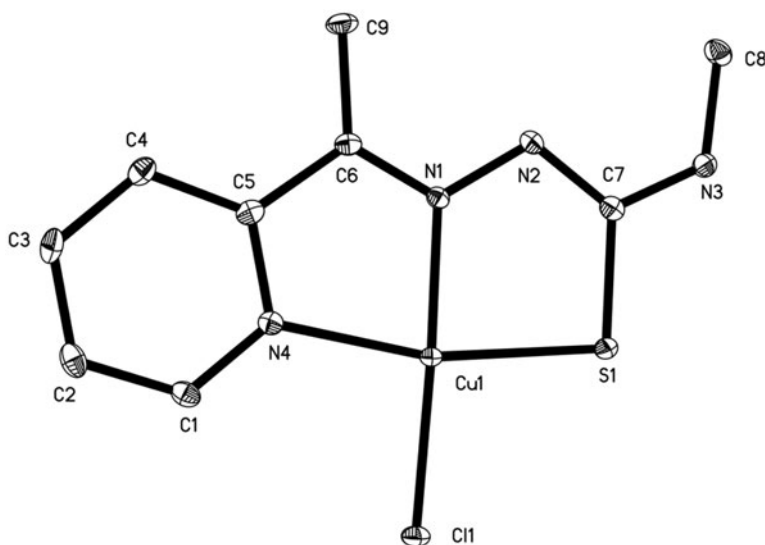


Figure 1. Thermal ellipsoid plot of **1** (30% probability; hydrogens omitted for clarity).

sulfur from $4ML^-$ at Cu1–N4 2.015(2) Å, Cu1–N1 1.958(2) Å, and Cu1–S1 2.242(7) Å, as well as Cl^- at Cu1–Cl1 2.231(7) Å to construct a basal plane. The basal atoms (N1, N4, S1, and Cl1) deviated from their mean plane by ca. 0.0007 Å and Cu1 is displaced out of the plane by ca. 0.0481 Å. There were no solvent molecules in **1**. However, **1** is still neutral, for the deprotonated thiosemicarbazone arm. Exact mass was detected by MS method, which indirectly proved the removal of the H atoms of **1**.

Two adjacent $[Cu(4ML)Cl]$ units were connected by a weak bond through N_{amino} of $4ML^-$ ligand of one mononuclear unit occupying the apical position of Cu center of the other unit with longer distances [Cu1–N2 3.341 Å], thus forming the $[Cu(4ML)Cl]$ dimer. The dimeric units were further linked by distinct π – π stacking between pyridyl ring and the conjugated thiosemicarbazone arm from neighboring $4ML^-$ in a head-to-tail style with the shortest atom-to-atom ($C1 \cdots C6\#$) at 3.344 Å (see figure 2), thus enhancing the stability of the complex. Crystal data and experimental details are listed in table 1. Interatomic distances and bond angles are compiled in table 2.

3.2. DNA cleavage activities

To check DNA cleavage activity of **1**, plasmid pUC19 was used as substrate. As shown in the panel (a) of figure 3, the supercoiled form (SC) of the plasmid was reduced while the nicked circular form (NC) became apparent gradually, as the concentration of **1** increased. When the concentration of **1** reached 400 μM in the presence of H_2O_2 , only NC band was observed, indicating almost all of the SC plasmid had been cleaved by **1**.

To explore the possible DNA damage mechanism of **1**, various DNA cleavage experiments were carried out by adding DMSO (hydroxyl radical scavenger), NaN_3 (singlet oxygen quencher), SOD (superoxide scavenger), EDTA (chelating agent), L-histidine (singlet oxygen quencher), and KI (hydrogen peroxide scavenger), respectively. No obvious inhibition effect was observed for **1** in the presence of SOD (lane 5 in the panel (b) of figure 3),

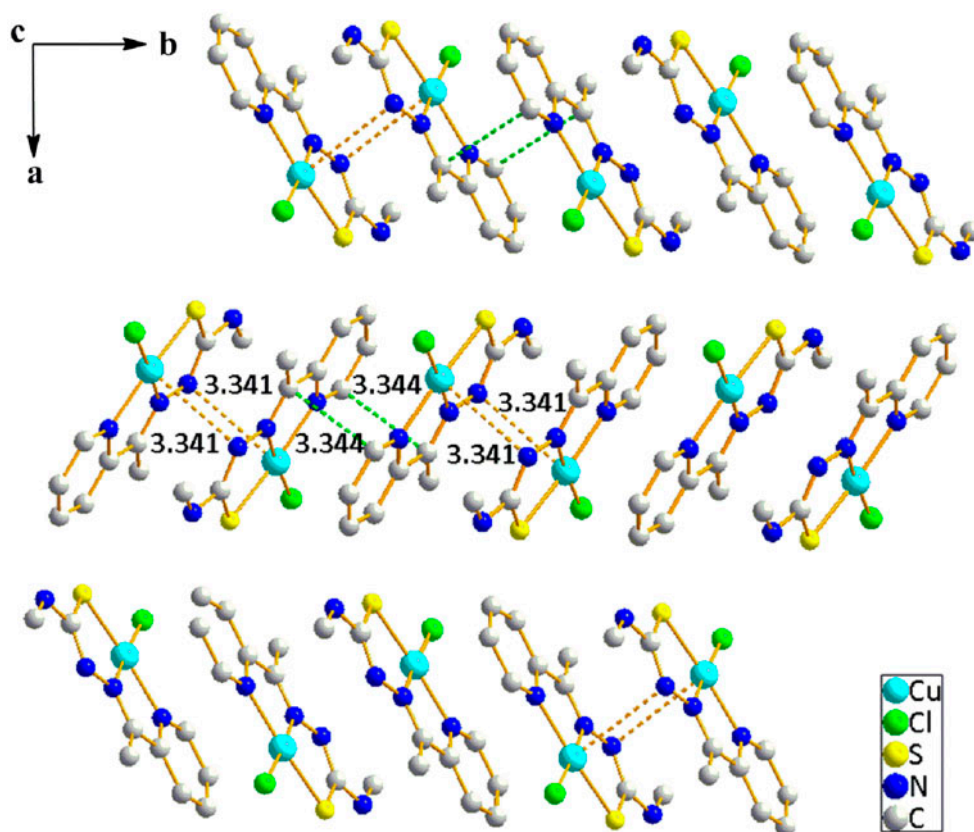


Figure 2. The packing diagram of **1** viewed along the *c*-axis showing extensive π - π interaction.

which excluded the possibility of DNA cleavage by superoxide. However, DMSO (lane 3), NaN_3 (lane 4), L-histidine (lane 7), and KI (lane 8) significantly diminished the cleavage activity of **1**, which were indicative of the involvement of hydroxyl radical and singlet oxygen in the cleavage process. EDTA (lane 6), a metal-specific chelating agent that strongly binds to metal ion forming a stable complex, efficiently inhibited the DNA cleavage activity of **1**, suggesting that copper played a key role in the DNA cleavage. Such observations imply that DNA cleavage may be attributed to the involvement of hydroxyl radical and singlet oxygen mechanism.

3.3. Complex **1** inhibited proliferation and growth in a variety of tumor cells

We then examined the cytotoxicity of **1** to tumor cells. Previously, a series of HAM4M ((*Z*)-2-(amino(pyridin-2-yl)methylene)-*N*-methylhydrazinecarbothioamide) metal complexes, including $[\text{Cu}(\text{Am4M})(\text{OAc})] \cdot \text{H}_2\text{O}$ (**2**), $[\text{Zn}(\text{HAM4M})\text{Cl}_2]$, $[\text{Zn}_2(\text{Am4M})_2\text{Br}_2]$, and $[\text{Zn}_2(\text{Am4M})_2(\text{OAc})_2] \cdot 2\text{MeOH}$, were reported and their structure-activity relationship was analyzed [47]. Complex **2**, based on TSC core and copper, showed a significant inhibition activity on cancer cell proliferation. Comparing **1** with **2**, $-\text{NH}_2$ to C6 position of TSC core

Table 1. Summary of crystal data for [Cu(4ML)Cl] (1).

Complex	C ₉ H ₁₁ ClCuN ₄ S (1)
<i>M</i> r	306.27
Space group	<i>P</i> 2 ₁ / <i>c</i>
<i>a</i> , Å	7.9769(2)
<i>b</i> , Å	15.8242(5)
<i>c</i> , Å	9.1259(2)
α , °	90
β , °	91.974(2)
γ , °	90
<i>V</i> , Å ³	1151.26(5)
<i>Z</i>	4
ρ_{calcd} , g cm ⁻³	1.767
<i>T</i> , K	293(2)
μ , mm ⁻¹	2.286
<i>F</i> (0 0 0)	620
Crystal size, mm	0.15 × 0.12 × 0.12
θ limits, °	2.58–25.24
Reflections collected	5101
Independent reflections	2079 [<i>R</i> _{int} = 0.0241]
Completeness to θ (%)	99.9
Data/restraints/parameters	2079 / 0 / 149
Goodness of fit on <i>F</i> ²	1.050
<i>R</i> ₁ [<i>I</i> > 2 σ (<i>I</i>)]	0.0272

Table 2. Bond lengths [Å] and angles [°] for 1.

Cu1–N1	1.958(2)	Cu1–N4	2.015(2)
Cu1–Cl1	2.2312(7)	Cu1–S1	2.2419(7)
N1–Cu1–N4	80.44(9)	C7–S1–Cu1	94.60(9)
N1–Cu1–Cl1	176.73(6)	C6–N1–Cu1	117.85(17)
N4–Cu1–Cl1	97.51(6)	N2–N1–Cu1	123.18(16)
N1–Cu1–S1	85.11(6)	C1–N4–Cu1	128.01(18)
N4–Cu1–S1	165.38(6)	C5–N4–Cu1	112.71(17)
Cl1–Cu1–S1	96.81(3)		

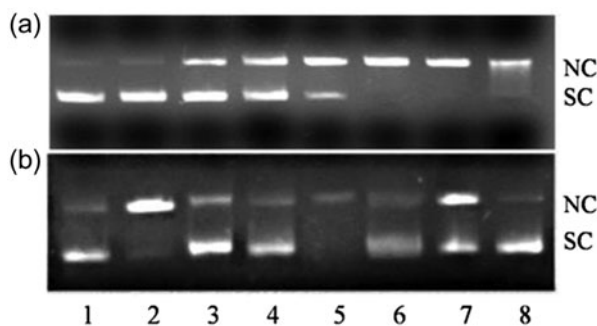
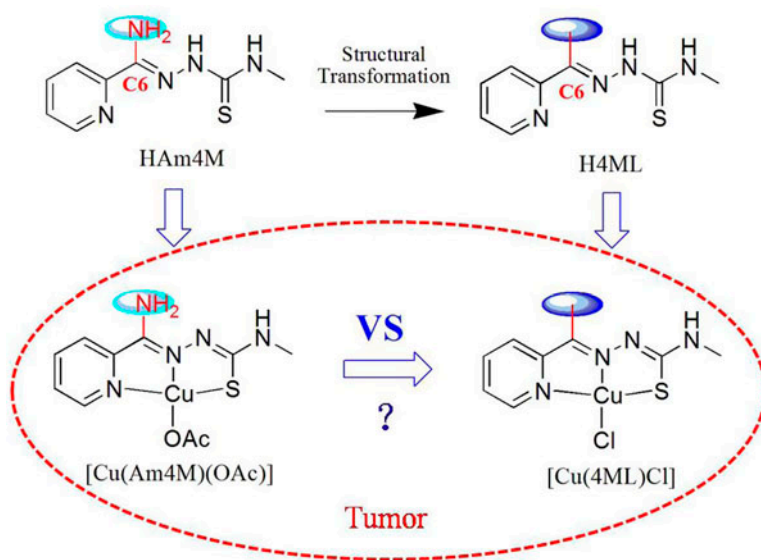


Figure 3. Gel electrophoresis separations showing the cleavage of SC pUC19 DNA (100 ng) by 1 (a) Lane 1: DNA control. Lane 2: DNA + H₂O₂ (1.2 mM). Lanes 3–8: DNA + 1 (100, 200, 300, 400, 500, and 600 μM, respectively) + H₂O₂ (1.2 mM). (b) Lane 1: DNA control. Lane 2: DNA + 1 (400 μM) + H₂O₂ (1.2 mM). Lane 3: DNA + 1 (400 μM) + H₂O₂ (1.2 mM) + DMSO (5 μL). Lane 4: DNA + 1 (400 μM) + H₂O₂ (1.2 mM) + NaN₃ (125 μM). Lane 5: DNA + 1 (400 μM) + H₂O₂ (1.2 mM) + SOD (6 u). Lane 6: DNA + 1 (400 μM) + H₂O₂ (1.2 mM) + EDTA (500 μM). Lane 7: DNA + 1 (400 μM) + H₂O₂ (1.2 mM) + L-histidine (125 μM). Lane 8: DNA + 1 (400 μM) + H₂O₂ (1.2 mM) + KI (500 μM).



Scheme 2. Structural modifications.

in **2** was changed into $-\text{CH}_3$ to that in **1** (scheme 2). Interestingly, ESI-MS revealed that **1** and **2** present similar ionic entity $[\text{Cu}(\text{L})]^+$ in MeOH solution. Various human tumor cells (HeLa, HepG-2, and SGC-7901 cell lines) were treated by **1** at 0, 1.25, 2.5, 5, and 10 μM for 48 h. MTT assay indicated that treatment with **1** resulted in a significant reduction in cell viability of these three tumor cell lines (table 3). The IC_{50} values by **1** were 3.2 ± 0.7 , 7 ± 1 , and 5 ± 1 μM against HeLa, HepG-2, and SGC-7901 cell lines for 48 h while 10 ± 2 , 25 ± 3 , and 7 ± 3 μM by cisplatin. In comparison, both free copper ion and H4ML showed poorer growth inhibition activities than **1**, which indicated that chelation of H4ML with copper ion was essential for anticancer activities of **1**. Complex **1** was nearly four times as cytotoxic to HepG-2 cells as cisplatin. Complex **1** showed much stronger cytotoxicity than **2** (up to 6.4 folds) in tested cell lines (table 3), suggesting that the $-\text{CH}_3$ substitution of the $-\text{NH}_2$ on the C6 position of TSC arm could increase the activity markedly.

We did further research on the antitumor activities in HeLa cells as it seemed that HeLa cells were the most sensitive to **1** among tested cell lines. Dose- and time-response of **1** (0, 1.25, 2.5, 5, and 10 μM) against HeLa cells by MTT assay are shown in figure 4. The IC_{50}

Table 3. IC_{50} values (μM) obtained with different cell lines for 48 h.^a

Complex	Molecular formula	Antitumor activity IC_{50} (μM)		
		HeLa	HepG-2	SGC-7901
Ion	Cu	>50	>50	>50
Ligand	H4ML	15 ± 3	19 ± 5	>50
1	$[\text{Cu}(4\text{ML})\text{Cl}]$	3.2 ± 0.7	7 ± 1	5 ± 1
2	$[\text{Cu}(\text{Am4M})(\text{OAc})] \cdot \text{H}_2\text{O}$	20 ± 2	11 ± 1	16 ± 2
Cisplatin	$\text{Pt}(\text{NH}_3)_2\text{Cl}_2$	10 ± 2	25 ± 3	7 ± 3

^aThe IC_{50} values of **2** were adopted from our previous report [47].

values for 24, 48, and 72 h treatments were 8 ± 1 , 3.2 ± 0.7 , and 1.2 ± 0.4 μM , respectively. The results indicated that **1** was cytotoxic to HeLa cells and inhibited the growth of cells in a dose- and time-dependent manner. Furthermore, clonogenic assay was used to measure the antiproliferative effects of **1** on HeLa cells. As shown in figure 5, the number of colony-forming cells was 87.3, 59.8, and 34.9% of untreated controls at dosages of 0.3125, 0.625, and 1.25 μM , suggesting that **1** inhibited clonogenic growth of HeLa cells in a dose-dependent manner. No colony could be observed at 2.5 and 5 μM of **1**, consistent with that of MTT assay, indicating that **1** could effectively suppress HeLa cell growth and proliferation.

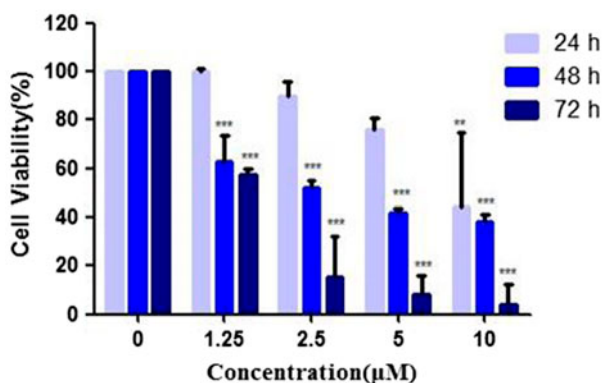


Figure 4. Cell viability of HeLa cells after drug treatment (0, 1.25, 2.5, 5, and 10 μM) for 24, 48, and 72 h by MTT assay. The IC_{50} values at 24, 48, and 72 h were 8 ± 1 , 3.2 ± 0.7 , and 1.2 ± 0.4 μM for **1**, respectively. The results were expressed as the Mean \pm SD ($n = 3$). * $p < 0.05$, ** $p < 0.01$, *** $p < 0.001$ compared with the control group.

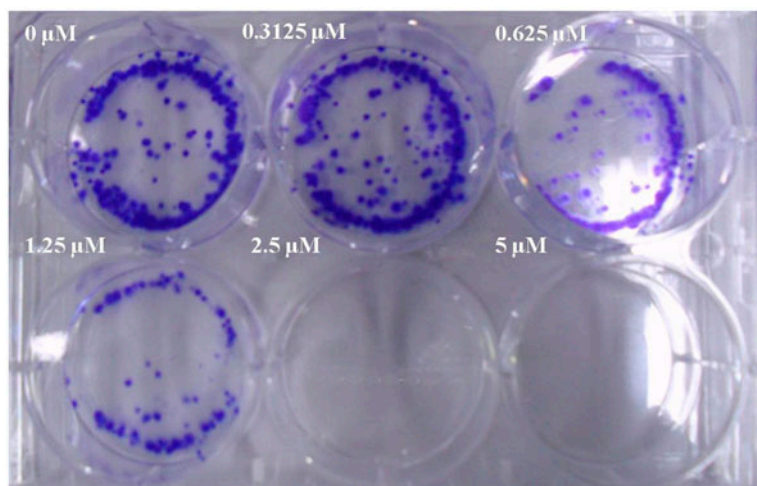


Figure 5. Clonogenic capacity in HeLa cells detected by colony-forming assay (crystal violet staining). Cells were treated by varied concentrations (0, 0.3125, 0.625, 1.25, 2.5, and 5 μM , respectively) of **1** for 24 h and incubated for two weeks total. The cloning efficiency (%) was significantly decreased in treated cells compared with untreated cells.

3.4. Complex 1 induced apoptosis in HeLa cells

To determine whether reduction of proliferation capacity and cell viability of the HeLa cells induced by **1** was associated with cell apoptosis, cells were treated with **1** at 0, 5, 10, and 20 μM for 24 h. Apoptotic cells were assessed using both qualitative and quantitative methods. Hoechst 33342 staining and Annexin V-FITC/PI binding assays were performed. In Hoechst 33342 staining assay, morphological changes were observed, and we found that increasing doses of **1** resulted in characteristic features of apoptosis including cell shrinkage and nuclear changes followed by gradual rounding of cells and lifting off the culture plate. Photographs of treated cells shown in figure 6 demonstrated that the number of apoptosis cells increased in a dose-dependent manner. In addition, it showed that there was an increased fraction of Annexin V-FITC (early apoptosis) and Annexin V-FITC/PI (late apoptosis) in HeLa cells [figure 7(a)]. Annexin V-FITC/PI staining data indicated that percentage of early apoptosis was 3.2, 31.5, 54.6, and 66.4% [figure 7(b)] with the increasing dosage of **1**, respectively. These data suggested that **1** caused apoptotic induction in HeLa cells.

3.5. Complex 1 increased ROS production in HeLa cells

DCFH-DA was used as a probe for intracellular oxidative stress, and ROS production was evaluated by flow cytometry after treatment with **1** at 0, 5, 10 and 20 μM for 24 h. In HeLa cells, the increased production of ROS was detected in treatment groups and cells turned round at higher drug concentration (figure 8). ROS have been implicated in the induction or enhancement of apoptosis and are produced upon stress stimulation such as UV, γ -irradiation, or cytotoxic drugs. The effect caused by ROS generation has been considered as a possible anticancer strategy.

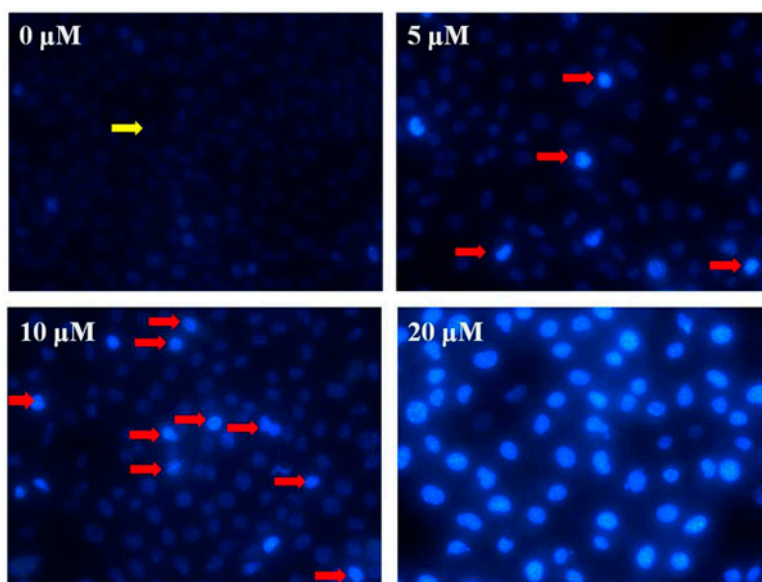


Figure 6. Representative images of cell morphology: Hoechst 33342 staining detected morphological changes in HeLa cells after treatment by **1** (0, 5, 10, and 20 μM) for 24 h. Complex **1** caused nuclei to be condensed and fragmented. Yellow arrows point out normal cells, while red arrows for apoptotic cells (see <http://dx.doi.org/10.1080/00958972.2014.979811> for color version).

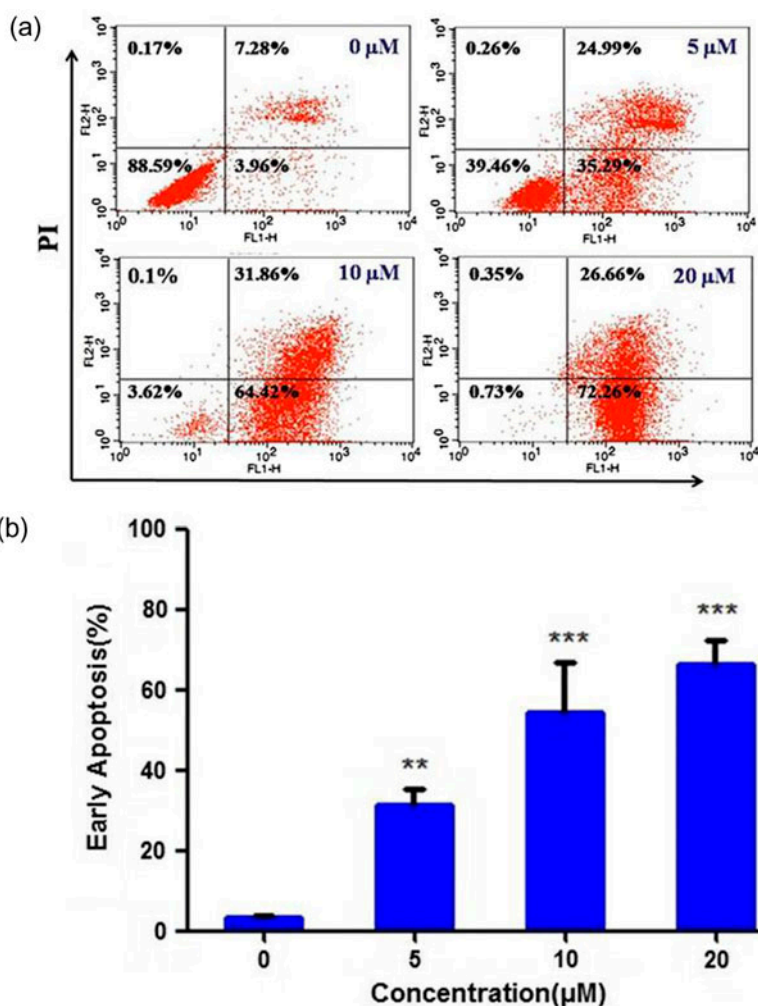


Figure 7. Apoptosis induced by **1** against HeLa cells: (a) the image of apoptosis in cells after treatment for 24 h at 0, 5, 10, and 20 μM using Annexin V- FITC/PI staining and (b) statistical analysis result of early apoptosis in cells. * $p < 0.05$, ** $p < 0.01$, *** $p < 0.001$ compared with the control group.

3.6. Complex 1 caused DNA damage of HeLa cells

Comet assay was applied to detect DNA fragmentation, which has been widely used to measure oxidative damage of human cellular DNA in relation to diseases. Oxidative damage induces primary DNA lesions including single-strand breaks, double-strand breaks, incomplete excision repair sites, and alkali labile sites that can be converted into DNA single-strand breaks. Cells with increased DNA damage display increased migration of chromosomal DNA from the nucleus toward the anode, which resembles a comet-like tail. In contrast, untreated cells have a nearly round and healthy looking nucleus. HeLa cells were incubated with **1** at 0, 5, 10, and 20 μM for 24 h, and data from comet assay were calculated in the term of the "Olive Tail Moment" of comets. The results (figure 9) indicated that **1** induced severe DNA fragmentation in HeLa cells in a dose-dependent manner.

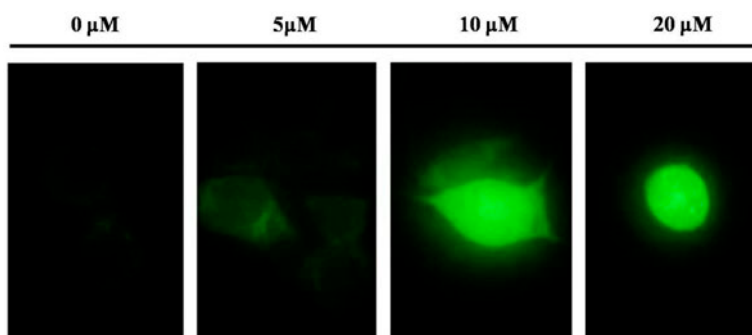


Figure 8. Generation of ROS induced by **1** in HeLa cells. Cells were treated with 0, 5, 10, and 20 μM of **1** for 24 h.

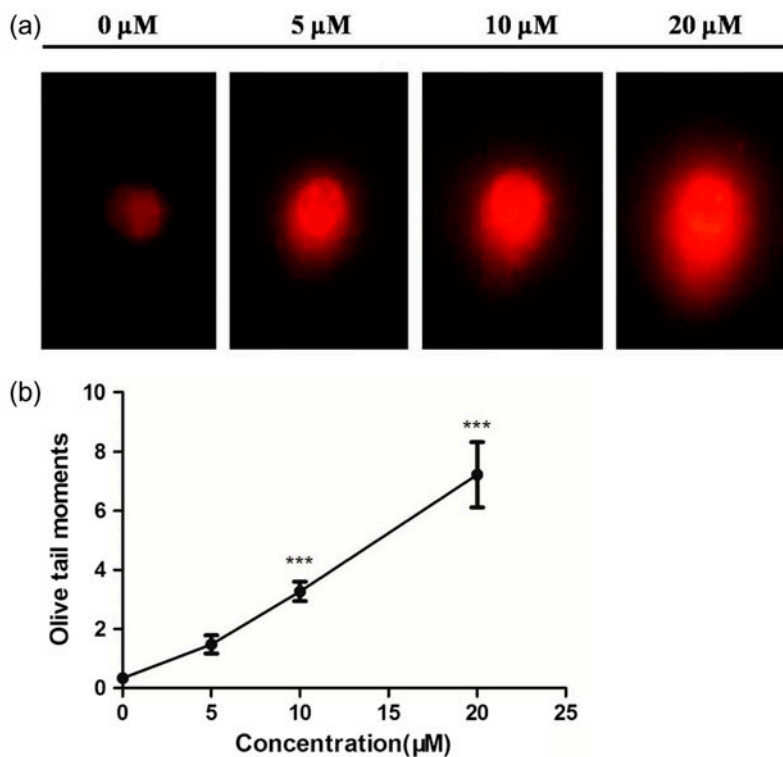


Figure 9. Complex **1** induced DNA damage of HeLa cells and the DNA fragmentation measured by the comet assay. HeLa cells were treated with varied concentrations of **1** (0, 5, 10, and 20 μM) for 24 h: (a) image of DNA damage detected by comet assay in HeLa cells after treatment with **1** and (b) statistical analysis results of comet assay to assess DNA damage calculated in the term of the "Olive Tail Moment" of comets. Data represent the mean \pm SD of three-independent experiments. * $p < 0.05$, ** $p < 0.01$, *** $p < 0.001$, compared with the control group.

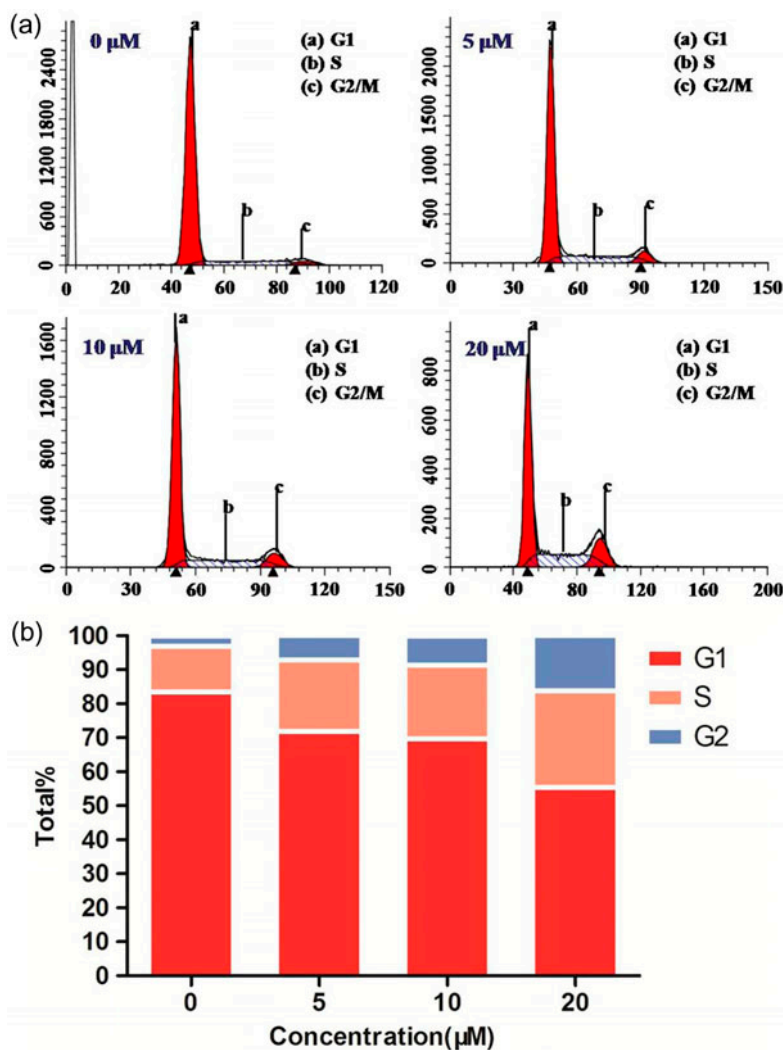


Figure 10. Effect of **1** on cell cycle progression in HeLa cells. The cell cycle distribution of HeLa cells was detected by flow cytometric analysis of DNA content after treatment with **1** at 0, 5, 10, and 20 μM for 24 h: (a) image of cell cycle distribution in HeLa cells treated with **1** and (b) statistical analysis about DNA content analysis in HeLa cell cycle distribution.

3.7. Complex 1 influence on HeLa cell cycle distribution

In order to identify whether **1** could have an influence on DNA synthesis and other cell cycle processes, DNA content profiles of HeLa cells were analyzed by flow cytometry after treatment with **1** (0, 5, 10, and 20 μM) for 24 h. As shown in figure 10, the population of cells in S phase changed from 13.39% (in control cells) to 21.05, 21.67, and 28.57% at 5, 10, and 20 μM of **1** while 3.14% to 7.20, 8.63, and 16.09% in G2 phase. Generally speaking, cell numbers in both S and G2 phases had a significant increasing trend by treatments with **1**, and more obvious changes occurred in G2 phase than S phase. The accumulation of

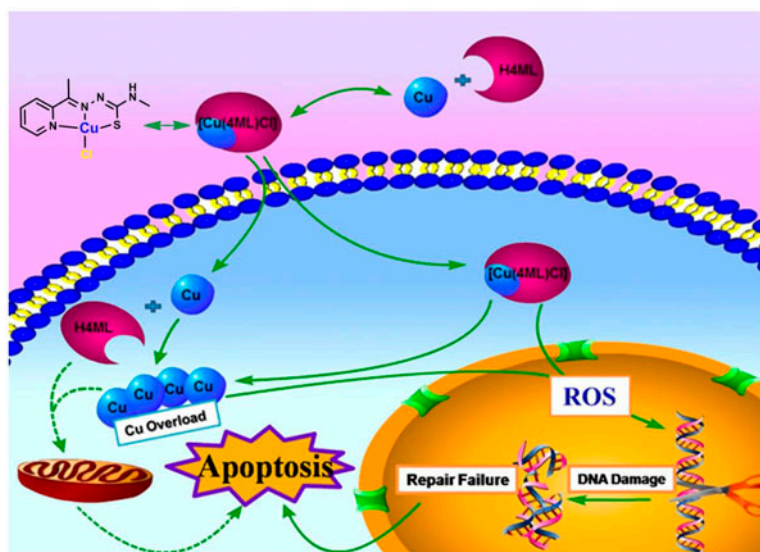


Figure 11. Potential mechanism for **1** in HeLa cells.

cells in the two phases of the cell cycle suggests that **1** could delay or inhibit cell cycle progression through a possible arrest at S and G2 phases. S phase is associated with DNA synthesis and plays a crucial role in cell cycle progression, and in G2 phase, proteins, and RNA molecules are synthesized, preparing the conditions for entry into mitosis. Therefore, the role of **1** in growth inhibition and proliferation hindering of HeLa cells could be associated with the cell cycle arrest.

4. Conclusion

[Cu(4ML)Cl] (**1**) was prepared and characterized using spectroscopic and X-ray diffraction methods. X-ray crystal analysis indicated that **1** is a mononuclear unit with square planar geometry similar to cisplatin. The complex displayed excellent inhibitory activities against various tumor cells, especially HeLa cells. Cell viability assay presented the IC_{50} values of **1** in HeLa, HepG-2, and SGC-7901 cells ranging from about 3 to 7 μM , which is lower than cisplatin in all tested cell lines. Among them, HeLa cell line was most sensitive to **1**. Compared to some other copper complexes with non-TSCs [48, 49] or TSCs [47] ligands, **1** exhibited higher growth inhibition activities against tumor cells, probably owing to introduction of thiosemicarbazone group, or modification of functional substituent (see scheme 2); such interesting observation warrants further investigation on the copper complex. Results of Hoechst 33342 staining and Annexin V-FITC/PI showed that **1** induced apoptosis of HeLa cells in a dose-dependent manner. The amount of intracellular ROS was elevated with increasing concentration of **1**. Complex **1** was capable of cleaving DNA through an oxidative DNA damage pathway, consistent with the result of comet assay showing that **1** induced severe DNA fragmentation (figure 11). ROS-induced DNA damage is important in the regulation of cell death and survival. Furthermore, **1** could induce S-phase and

G2-phase arrests in HeLa cells. It is likely that DNA damage by **1** directly affects DNA replication, transcription, and protein synthesis. Thus, it is worthy of further investigation on this copper complex as an antitumor candidate.

Supplementary material

Figure S1 gives the ESI-MS spectrum of $[\text{Cu}(\text{4ML})]^+$. Crystallographic data for **1** has been deposited at the Cambridge Crystallographic Data Center (CCDC) No. 917282. The data can be obtained free of charge from CCDC via www.ccdc.cam.ac.uk/data_request/cif, by e-mailing data_request@ccdc.cam.ac.uk or by contacting the Cambridge Crystallographic Data Center, 12 Union Road, Cambridge CB2 1E Z, UK; Fax: +44 (0)122 3 336033.

Funding

This work was supported by National Natural Science Foundation of China [grant number 21371135] and Tianjin Municipal Natural Science Foundation [grant number 13JCZDJC28200], [grant number 11JCYBJC14900].

References

- [1] L. Ronconi, P.J. Sadler. *Coord. Chem. Rev.*, **251**, 1633 (2007).
- [2] D.R. Williams. *Chem. Rev.*, **72**, 203 (1972).
- [3] Z.J. Guo, P.J. Sadler. *Angew. Chem. Int. Ed.*, **38**, 1513 (1999).
- [4] L.R. Kelland, N.P. Farrell, S. Spinelli. In *Uses of Inorganic Chemistry in Medicine*, N.P. Farrell (ed), pp. 109–134, The Royal Society of Chemistry, Cambridge (1999).
- [5] M.J. Piccart, H. Lamb, J.B. Vermorken. *Ann. Oncol.*, **12**, 1195 (2001).
- [6] G.Y. Park, J.J. Wilson, Y. Song, S.J. Lippard. *Proc. Natl. Acad. Sci. USA*, **109**, 11987 (2012).
- [7] S. Padhyé, G.B. Kauffman. *Coord. Chem. Rev.*, **63**, 127 (1985).
- [8] J. Easmon, G. Pürstinger, G. Heinisch, T. Roth, H.H. Fiebig, W. Holzer, W. Jäger, M. Jenny, J. Hofmann. *J. Med. Chem.*, **44**, 2164 (2001).
- [9] W. Kaim, J. Rall. *Angew. Chem. Int. Ed.*, **35**, 43 (1996).
- [10] S. Buschmann, E. Warkentin, H. Xie, J.D. Langer, U. Ermler, H. Michel. *Science*, **329**, 327 (2010).
- [11] H.M. Alvarez, Y. Xue, C.D. Robinson, M.A. Canalizo-Hernandez, R.G. Marvin, R.A. Kelly, A. Mondragon, J.E. Penner-Hahn, T.V. O'Halloran. *Science*, **327**, 331 (2010).
- [12] P. Gourdon, X.Y. Liu, T. Skjærringe, J.P. Morth, L.B. Møller, B.P. Pedersen, P. Nissen. *Nature*, **475**, 59 (2011).
- [13] N.J. Robinson. *Nature*, **475**, 41 (2011).
- [14] A.R. Reddi, V.C. Culotta. *Cell*, **152**, 224 (2013).
- [15] G. Gupta-Elera, A.R. Garrett, R.A. Robison, K.L. O'Neill. *Eur. J. Cancer Prev.*, **21**, 155 (2012).
- [16] C.Z. Xie, M.M. Sun, S.H. Li, X.T. Zhang, X. Qiao, Y. Ouyang, J.Y. Xu. *J. Coord. Chem.*, **66**, 3891 (2013).
- [17] T.T. Xing, S.H. Zhan, Y.T. Li, Z.Y. Wu, C.W. Yan. *J. Coord. Chem.*, **66**, 3149 (2013).
- [18] M. Komatsu, T. Sumizawa, M. Mutoh, Z.S. Chen, K. Terada, T. Furukawa, X.L. Yang, H. Gao, N. Miura, T. Sugiyama, S. Akiyama. *Cancer Res.*, **60**, 1312 (2000).
- [19] H. Miyashita, Y. Nitta, S. Mori, A. Kanzaki, K. Nakayama, K. Terada, T. Sugiyama, H. Kawamura, A. Sato, H. Morikawa, K. Motegi, Y. Takebayashi. *Oral Oncol.*, **39**, 157 (2003).
- [20] W.X. Hu, W. Zhou, C.N. Xia, X. Wen. *Bioorg. Med. Chem. Lett.*, **16**, 2213 (2006).
- [21] B.M. Zegliss, V. Divilov, J.S. Lewis. *J. Med. Chem.*, **54**, 2391 (2011).
- [22] A.E. Liberta, D.X. West. *Biometals*, **5**, 121 (1992).
- [23] H. Beraldo, D. Gambino. *Mini. Rev. Med. Chem.*, **4**, 159 (2004).
- [24] A.G. Quiroga, C. Navarro Ranninger. *Coord. Chem. Rev.*, **248**, 119 (2004).
- [25] S. Halder, S.M. Peng, G.H. Lee, T. Chatterjee, A. Mukherjee, S. Dutta, U. Sanyal, S. Bhattacharya. *New J. Chem.*, **32**, 105 (2008).
- [26] M. Belicchi-Ferrari, F. Bisceglie, C. Casoli, S. Durot, I. Morgenstern-Badarau, G. Pelosi, E. Pilotti, S. Pinelli, P. Tarasconi. *J. Med. Chem.*, **48**, 1671 (2005).
- [27] G.K. Walkup, S.C. Burdette, S.J. Lippard, R.Y. Tsien. *J. Am. Chem. Soc.*, **122**, 5644 (2000).

- [28] D.K. Sau, R.J. Butcher, S. Chaudhuri, N. Saha. *Mol. Cell Biochem.*, **253**, 21 (2003).
- [29] A.P. Rebolledo, G.M. de Lima, L.N. Gambi, N.L. Speziali, D.F. Maia, C.B. Pinheiro, J.D. Ardisson, M.E. Cortes, H. Beraldo. *Appl. Organomet. Chem.*, **17**, 945 (2003).
- [30] N.C. Kasuga, K. Sekino, M. Ishikawa, A. Honda, M. Yokoyama, S. Nakano, N. Shimada, C. Koumo, K. Nomiya. *J. Inorg. Biochem.*, **96**, 298 (2003).
- [31] Z. Afrasiabi, E. Sinn, J.N. Chen, Y.F. Ma, A.L. Rheingold, L.N. Zakharov, N. Rath, S. Padhye. *Inorg. Chim. Acta*, **357**, 271 (2004).
- [32] Z. Afrasiabi, E. Sinn, S. Padhye, S. Dutta, S. Padhye, C. Newton, C.E. Anson, A.K. Powell. *J. Inorg. Biochem.*, **95**, 306 (2003).
- [33] D. Kovala-Demertzi, M.A. Demertzis, J.R. Miller, C.S. Frampton, J.P. Jasinski, D.X. West. *J. Inorg. Biochem.*, **92**, 137 (2002).
- [34] A.G. Quiroga, J.M. Pérez, I. López-Solera, J.R. Masaguer, A. Luque, P. Román, A. Edwards, C. Alonso, C. Navarro-Ranninger. *J. Med. Chem.*, **41**, 1399 (1998).
- [35] I. Đilović, M. Rubčić, V. Vrdoljak, S. Kraljević Pavelić, M. Kralj, I. Piantanidab, M. Cindric. *Bioorg. Med. Chem.*, **16**, 5189 (2008).
- [36] X. Du, C. Guo, E. Hansell, P.S. Doyle, C.R. Caffrey, T.P. Holler, J.H. McKerrow, F.E. Cohen. *J. Med. Chem.*, **45**, 2695 (2002).
- [37] D.B. Lovejoy, D.R. Richardson. *Blood*, **100**, 666 (2002).
- [38] J. Easmon, G. Heinisch, W. Holzer, B. Rosenwirth. *J. Med. Chem.*, **35**, 3288 (1992).
- [39] D.L. Klayman, J.F. Bartosevich, T.S. Griffin, C.J. Mason, J.P. Scovill. *J. Med. Chem.*, **22**, 855 (1979).
- [40] B. Ma, B.C. Goh, E.H. Tan, K.C. Lam, R. Soo, S.S. Leong, L.Z. Wang, F. Mo, A.T. Chan, B. Zee, T. Mok. *Invest. New Drugs*, **26**, 169 (2008).
- [41] A.I. Matesanz, P. Souza. *Mini. Rev. Med. Chem.*, **9**, 1389 (2009).
- [42] D.X. West, H. Gebremedhin, R.J. Butcher, J.P. Jasinski. *Transition Met. Chem.*, **20**, 84 (1995).
- [43] E. Bermejo, R. Carballo, A. Castiñeiras, R. Domínguez, A.E. Liberta, C. Maichle-Mössmer, M.M. Salberg, D.X. West. *Eur. J. Inorg. Chem.*, **6**, 965 (1999).
- [44] E. Bermejo, R. Carballo, A. Castiñeiras, R. Domínguez, C. Maichle-Mössmer, J. Strähle, D.X. West. *Polyhedron*, **18**, 3695 (1999).
- [45] G.M. Sheldrick. *SHELXS-97, Program of the Solution of Crystal Structure*, University of Göttingen, Germany (1997).
- [46] G.M. Sheldrick. *SHELXL-97, Program of the Refinement of Crystal Structure*, University of Göttingen, Germany (1997).
- [47] J. Shao, Z.Y. Ma, A. Li, Y.H. Liu, C.Z. Xie, Z.Y. Qiang, J.Y. Xu. *J. Inorg. Biochem.*, **136**, 13 (2014).
- [48] X. Qiao, Z.Y. Ma, C.Z. Xie, F. Xue, Y.W. Zhang, J.Y. Xu, Z.Y. Qiang, J.S. Lou, G.J. Chen, S.P. Yan. *J. Inorg. Biochem.*, **105**, 728 (2011).
- [49] X. Qiao, Z.Y. Ma, J. Shao, W.G. Bao, J.Y. Xu, Z.Y. Qiang, J.S. Lou. *BioMetals*, **27**, 155 (2014).